PHYSICAL REVIEW D **90,** 114019 (2014)

Hadroproduction of φ-mesons in the quark-gluon string model

G. H. Arakelyan,[1,*] C. Merino,[2,†] and Yu. M. Shabelski[3,‡]

[1]*A. Alikhanyan National Scientific Laboratory (Yerevan Physics Institute), Yerevan 0036, Armenia*
[2]*Departamento de Física de Partículas, Facultade de Física and Instituto Galego de Física de Altas Enerxías (IGFAE), Universidade de Santiago de Compostela, 15782 Santiago de Compostela, Galiza, Spain*
[3]*Petersburg Nuclear Physics Institute, NRC Kurchatov Institute, Gatchina, St. Petersburg 188350, Russia*

(Received 31 July 2014; published 16 December 2014)

We consider the experimental data on φ-meson production in hadron-nucleon collisions for a wide energy region. The quark-gluon string model quantitatively describes the spectra of secondary φ, as well as the ratios of φ/π^- and φ/K^- production cross sections.

DOI: 10.1103/PhysRevD.90.114019 PACS numbers: 25.75.Dw

I. INTRODUCTION

The quark-gluon string model (QGSM) [1,2], based on the dual topological unitarization (DTU), Regge phenomenology, and nonperturbative notions of QCD, has been used for already more than thirty years to successfully predict and describe many features of the hadronic processes in a wide energy range. In particular, the QGSM allows one to make quantitative predictions on the inclusive densities of different secondaries both in the central and beam fragmentation regions.

In the QGSM frame, high-energy hadron-nucleon collisions are considered as taking place via the exchange of one or several Pomerons. Each Pomeron is considered in DTU as a cylindrical diagram [Fig. 1(a)]. The cut [3] between Pomerons in a multi-Pomeron diagram results in elastic or diffraction dissociation processes, while the cut through one [Fig. 1(b)] or several [Fig. 1(c)] Pomerons corresponds to inelastic processes with multiple production of secondaries, the cut of every Pomeron leading to the production of two showers of secondaries.

This model has been successfully used for the description of multiparticle production processes in hadron-hadron collisions. The QGSM description of the production of secondaries (pseudoscalar mesons π and K), and of nucleons p, $\bar{p}$, which give the main contribution to mean multiplicity at different energies was obtained many years ago in [4,5] (see also [6,7]). Vector meson production was considered in [8–10]. The yields of hyperons, including the multistrange ones, have been described in [11,12].

In the present paper, we apply the QGSM formalism to the description of the spectra of vector φ-meson production in πp and Kp collisions, and of the ratios of yields φ/π^- and φ/K^- in pp collisions for a large scope of the initial energy going up to the RHIC and LHC ranges. The φ meson is a system of $s\bar{s}$ quarks with nonzero masses, which is rarely produced and thus can be sensitive to the production mechanism.

II. MESON PRODUCTION IN THE QGSM

In the QGSM the inclusive spectrum of a secondary hadron h is determined [1,2] by the convolution of the diquark, valence quark, and sea quark distributions, $u(x,n)$, in the incident particles, with the fragmentation functions, $G^h(z)$, of quarks and diquarks into the secondary hadron h. Both the distribution and the fragmentation functions are constructed using the Reggeon counting rules [13].

For a nucleon target, the inclusive rapidity, y, or Feynman-x, x_F, spectrum of a secondary hadron h has the form [1]

$$\frac{dn}{dy} = \frac{x_E}{\sigma_{\rm inel}} \cdot \frac{d\sigma}{dx_F} = \sum_{n=1}^{\infty} w_n \cdot \phi_n^h(x), \qquad (1)$$

where the functions $\phi_n^h(x)$ determine the contribution of diagrams with n cut Pomerons, w_n is the relative weight of

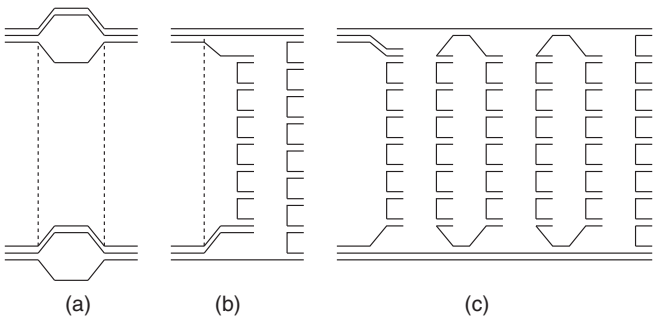

FIG. 1. (a) Cylindrical diagram representing a Pomeron exchange within the DTU classification (quarks are shown by solid lines), (b) a cut of the cylindrical diagram corresponding to the single-Pomeron exchange contribution to inelastic pp scattering, and (c) the cuts of the diagrams for the inelastic interaction of the incident proton with a target nucleon in a pp collision.

*argev@mail.yerphi.am
†merino@fpaxp1.usc.es
‡shabelsk@thd.pnpi.spb.ru

these diagrams, and the small diffraction dissociation contribution to φ-meson production processes has been neglected.

In the case of pp collisions,

$$\phi_n^h(x) = f_{qq}^h(x_+,n)\cdot f_q^h(x_-,n) + f_q^h(x_+,n)\cdot f_{qq}^h(x_-,n) + 2(n-1)\cdot f_s^h(x_+,n)\cdot f_s^h(x_-,n),$$
$$x_\pm = \frac{1}{2}\left[\sqrt{4m_T^2/s + x^2} \pm x\right], \tag{2}$$

where f_{qq}, f_q, and f_s correspond to the contributions of diquarks, valence quarks, and sea quarks, respectively. In the case of meson-nucleon collisions, the diquark contribution $f_{qq}^h(x_+,n)$ in Eq. (2) should be replaced by the valence antiquark contributions $f_{\bar{q}}^h(x_+,n)$.

The functions f_{qq}, f_q, $f_{\bar{q}}$, and $f_{\rm sea}$ are determined by the convolution of the diquark, quark, and antiquark distribution functions, $u(x,n)$, with the fragmentation functions to hadron h, $G^h(z)$, e.g.,

$$f_i^h(x_+,n) = \int_{x_+}^1 u_i(x_1,n) G_i^h(x_+/x_1)dx_1, \tag{3}$$

with $i = qq$-diquarks, $q,\bar{q}$, and sea quarks. The details of the model are presented in [1,2,4,5,11].

The classical Reggeon diagram technique [13,14] constructs the amplitude for hadron-hadron scattering at high energies of multi-Pomeron exchanges. In the case of supercritical Pomeron with

$$\alpha_P(t) = 1 + \Delta + \alpha'_P t, \qquad \Delta > 0, \tag{4}$$

one obtains the correct asymptotic behavior, $\sigma_{\rm tot} \sim \ln^2 s$. The one-Pomeron contribution to $\sigma_{hN}^{\rm tot}$ equals:

$$\sigma_P = 8\pi\gamma e^{\Delta\xi}, \qquad \xi = \ln s/s_0, \tag{5}$$

where γ is the Pomeron coupling, and σ_P rises with energy as s^Δ. To obey the s-channel unitarity, and the Froissart bound in particular, this contribution should be screened by the multi-Pomeron discontinuities. A simple quasieikonal treatment [15] yields

$$\sigma_{hN}^{\rm tot} = \sigma_P f(z/2), \qquad \sigma_{hN}^{\rm el} = \frac{\sigma_P}{C}[f(z/2) - f(z)], \tag{6}$$

where

$$f(z) = \sum_{k=1}^{\infty} \frac{1}{k\cdot k!}(-z)^{k-1} = \frac{1}{z}\int_0^z \frac{dx}{x}(1-e^{-x}),$$
$$z = \frac{2C\gamma}{\lambda}e^{\Delta\xi}, \qquad \lambda = R^2 + \alpha'_P\xi. \tag{7}$$

Here, R^2 is the radius of the Pomeron, and C is the quasieikonal enhancement coefficient (see [16]). At asymptotically high energies ($z \gg 1$), we obtain

$$\sigma_{hN}^{\rm tot} = \frac{8\pi\alpha'_P\Delta}{C}\xi^2, \qquad \sigma_{hN}^{\rm el} = \frac{4\pi\alpha'_P\Delta}{C^2}\xi^2, \tag{8}$$

according to the Froissart limit [17].

The values of Pomeron parameters were fixed [5] in 1986 on the base of a Regge fit [18] of high-energy hadron-nucleon scattering, by including into the analysis by then new data from colliders:

$$\Delta = 0.139, \qquad \alpha'_P = 0.21\ \text{GeV}^{-2},$$
$$\gamma_{pp} = 1.77\ \text{GeV}^{-2}, \qquad R^2_{pp} = 3.18\ \text{GeV}^{-2},$$
$$C_{pp} = 1.5, \qquad \gamma_{\pi p} = 1.07\ \text{GeV}^{-2},$$
$$R^2_{\pi p} = 2.48\ \text{GeV}^{-2}, \qquad C_{\pi p} = 1.65. \tag{9}$$

The error bars of the parameters are not presented, since they are strongly correlated. With this set of parameters of pp collision one obtains a value of $\sigma_{pp}^{\rm tot} \cong 94$ mb at the LHC energy of $\sqrt{s} = 7$ TeV, that is only slightly smaller than the experimental value $\sigma_{pp}^{\rm tot} = 98.3 \pm 2.8$ mb [19].

The cross sections of all inelastic processes corresponding to diagrams where $n \geq 1$ Pomerons are cutted can be calculated [15] with he help of the AGK cutting rules [3]:

$$\sigma_{hN}^{(n)} = \frac{\sigma_P}{n\cdot z}\left(1 - e^{-z}\sum_{k=1}^{n-1}\frac{z^k}{k!}\right). \tag{10}$$

The probabilities w_n in Eq. (1) are determined as

$$w^n = \sigma^n/(\sigma^{\rm tot} - \sigma^{\rm el}). \tag{11}$$

The average number of exchanged Pomerons in pp collisions $\langle n\rangle_{pp}$ slowly increases with the energy.

The distribution functions of quarks and diquarks in colliding particles were obtained in [20,21], and they are presented in the Appendix.

For the φ-meson production we use the following quark fragmentation functions [8], that were obtained by using the Reggeon counting rules and the simplest extrapolation [13]:

$$G_u^\varphi = G_d^\varphi = G_{\bar{u}}^\varphi = G_{\bar{d}}^\varphi = a_\varphi\cdot(1-z)^{\lambda-\alpha_R-2\alpha_\varphi+2}, \tag{12}$$

$$G_s^\varphi = G_{\bar{s}}^\varphi = a_\varphi\cdot(1-z)^{\lambda-\alpha_\varphi}. \tag{13}$$

The diquark fragmentation functions into φ mesons have the form

$$G_{uu}^\varphi = G_{ud}^\varphi = a_\varphi\cdot(1-z)^{\lambda+\alpha_R-2(\alpha_R+\alpha_\varphi)}, \tag{14}$$

where the parameter λ takes the value $\lambda = 0.5$, and the parameters $\alpha_R = 0.5$ and $\alpha_\varphi = 0.$ are the intercepts of the ρ and φ Regge trajectories, respectively. One has to note that the only unknown in this analysis is α_φ. This parameter α_φ represents the φ density in the central region of one Pomeron. In correspondence with what it has been well

established in the past for the corresponding parameters determining the yields of other particles, the value of this parameter is universal in the sense that it does not depend neither of the energy nor of the beam of the collision. Due to the significant systematic errors of some of the experimental data, to obtain the value of the parameter a_φ with the corresponding error bars from a global fit to all available experimental data is not possible. Thus, the value of the parameter a_φ, that sets the absolute normalization of the φ production cross section, has been fixed by simultaneously describing in a reasonable way most of the experimental data on φ production from pion and proton beams (see Sec. III). Thus, we use in our calculations the value of $a_\varphi = 0.11$, which gives a good description of most of those experimental data.

III. NUMERICAL RESULTS

In this section we first compare the QGSM calculations with the experimental data on φ inclusive cross sections in πp and pp collisions at different energies.

In Fig. 2 we present the experimental data for x_F spectra of φ mesons produced in $\pi^\pm p$ collisions at initial momenta of π mesons 93 [22], 100, 120 [23], and 140 GeV/c [24] (upper panel). The corresponding data for pion beam momenta 175, 200 [23], and 360 GeV/c [25] are shown in the lower panel of Fig. 2.

As it can be seen in the upper panel of Fig. 2, there is disagreement between the experimental data at 93, 140, 100, and 120 GeV/c. The corresponding QGSM calculations are also presented in Fig. 2. Thus, the x_F spectra of φ mesons produced in $\pi^\pm p$ collisions at energies 140 and 93 GeV/c are shown by full and dashed curves, respectively. The theoretical curves for 100 and 120 GeV/c are not presented in Fig. 2 due to the lack of space, but evidently they would be placed between the full and the dashed curves. The theoretical curves have been all calculated with $a_\varphi = 0.11$, and they are in good agreement with experimental data at both 93 and 140 GeV/c. The experimental data at 100 and 120 GeV/c [23] were obtained with the help by extrapolating Be target data by using linear A dependence, and they are systematically higher than other experimental data at even higher energies.

In the lower panel of Fig. 2, the data on φ-meson production at the higher energies of 175, 200, and 360 GeV/c are also presented. We see that the experimental data for these three energies are in agreement with the results of the theoretical calculations for the value $a_\varphi = 0.11$), and shown by full, dashed, and dashed-dotted curves, respectively. Here, the theoretical curves are in general agreement with the data, except for the small x_F region, where we predict a significant increase of $d\sigma/dx_F$ from 200 to 360 GeV/c that is not seen in the experimental data.

The QGSM description of the experimental data on the x_F dependence of $d\sigma/dx_F$ spectra of φ mesons in pp collision measured at 93 [22], 120, 200 [23], and 158 GeV/c [14,26], obtained with a value of $a_\varphi = 0.11$ is presented in Fig. 3. The full curve corresponds to the energy 93 GeV/c, the dashed curve to 158 GeV/c, and the dashed-dotted curve to 200 GeV/c. The agreement of the theoretical calculation with the data is reasonable at small x_F; at large x_F the experimental data falls down faster than the theory, except for the data at 93 GeV/c, when even at small x_F the agreement is not good. One can appreciate some contradiction between the data of φ-meson production in pp (Fig. 3) and those in πp (upper panel of Fig. 2)

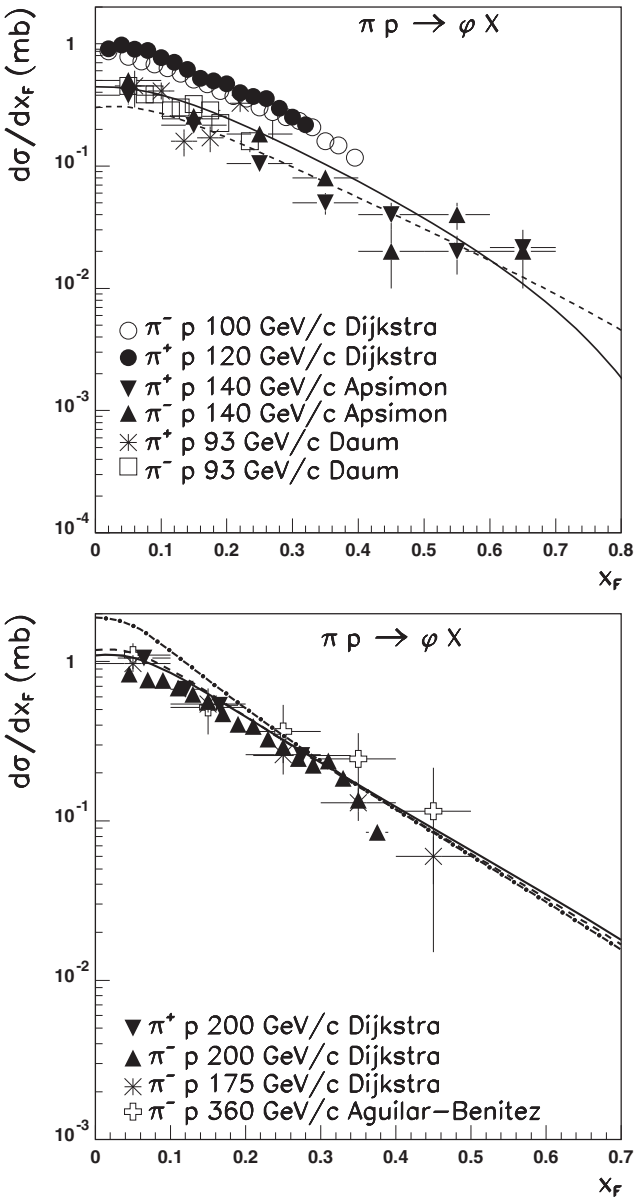

FIG. 2. Different experimental data on x_F spectra of φ mesons produced in $\pi^\pm p$ collisions at different energies [22–24], compared to the corresponding QGSM calculations (see the main text for the description of the different experimental data sets and theoretical curves).

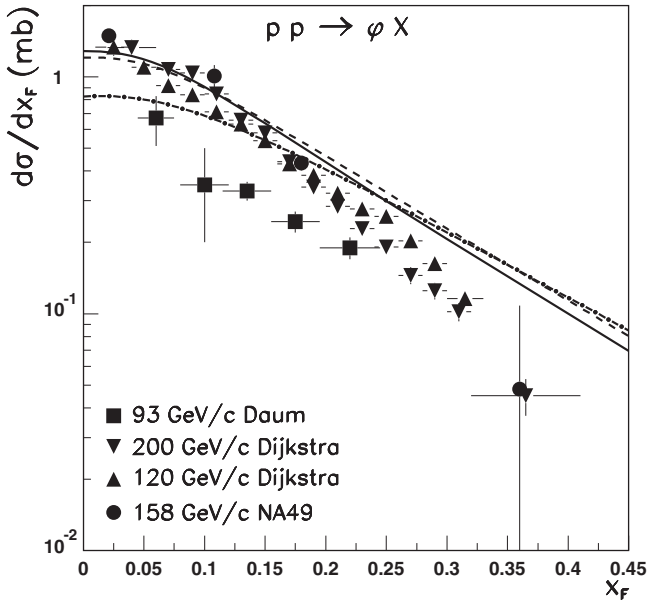

FIG. 3. The experimental data [14,22,23,26] on the x_F spectra of φ mesons produced in pp collisions at 93, 120, 158, and 200 GeV/c, compared to the corresponding QGSM calculations at 93, 158, and 200 GeV/c.

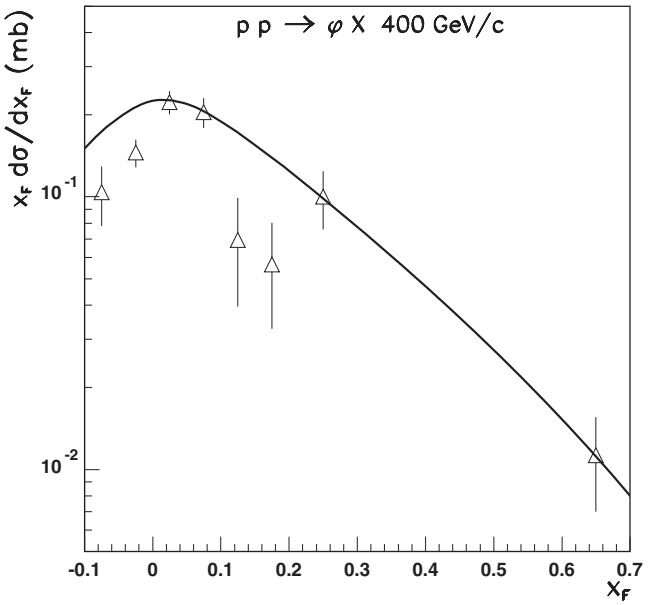

FIG. 4. The QGSM x_F spectra of φ mesons produced in pp collisions at 400 GeV/c compared to the experimental data [28].

collisions, obtained both by the same experiment [22]. Our results calculated at the NA49 Collaboration energy are in agreement with the Monte Carlo predictions obtained by using the LUCIAE model [27].

In Fig. 4, we compare the QGSM calculations to the experimental data on the inclusive spectra $x_F \cdot d\sigma/dx_F$ of φ mesons in pp collision at 400 Gev/c [28]. The agreement of theoretical curve ($a_\varphi = 0.11$) with the data is good.

In Fig. 5, the rapidity spectra dn/dy of φ-mesons production in pp collisions at 158 GeV/c [14,26] are compared to the QGSM calculation (full line). The agreement is quite reasonable. The predictions for the same spectra at the LHC energies of 7 TeV (dashed line) and 14 Tev (dashed-dotted line) are also presented.

Generally, the QGSM description of the experimental data in the considered energy region shown in Figs. 2–5 is consistent. The description of the large x_F region is rather good in the case of πp collisions, while for pp collisions there is not experimental point at $x_F > 0.35$, except for one point at 400 GeV/c that is in agreement with our curve. Due to the systematical uncertainties of some experimental results shown in Figs. 2–5, it is not possible to obtain the value of the parameter a_φ by standard fit procedure. After comparing our results with the available experimental data, we have taken the value $a_\varphi = 0.11$ as the most probable, and we have used this value for all the theoretical calculations presented in this paper.

The QGSM predictions have been always rather reliable for describing π-meson production up to the LHC energies [4,5,7]. Thus we have used the published calculations on π-meson yields to compute the ratios φ/π.

The spectra of kaons are presented in Fig. 6. We present the QGSM description of the experimental data on the inclusive spectra of K^+ (upper panel) and K^- (lower panel) mesons in pp collisions on a wide energy range from 100 GeV/c up to $\sqrt{s} = 200$ GeV [14,26,29]. The integrated over p_T RHIC data at $\sqrt{s} = 200$ GeV have been taken from [14,26].

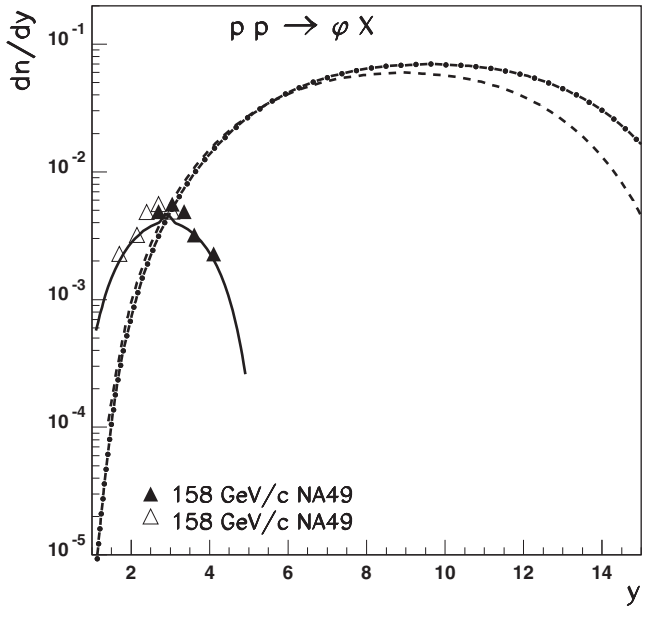

FIG. 5. The experimental data [28] on the y spectra dn/dy of φ mesons produced in pp collisions at 158 GeV/c, and the corresponding QGSM calculation (full line). The dashed and dashed-dotted lines correspond to QGSM predictions for LHC energies of 7 and 14 TeV, respectively.

We present the results of the QGSM calculations at the two different energies: 158 GeV/c ($\sqrt{s} = 17.3$ GeV), by solid curves, and RHIC energy ($\sqrt{s} = 200$ Gev), by dashed curves. In both cases, K^+ and K^- spectra, our curves are in reasonable agreement with the data. One has to note that some disagreement in the normalization of the experimental data by the NA49 Collaboration [14,26] and that of the data at 100 and 175 GeV/c [29] exists. Generally, the experimental spectra of both K^+ and K^- increase with the initial energy, what is in agreement with our calculations.

At very high energies ($\sqrt{s} = 900$ GeV and 7 Tev at LHC), φ-meson production was measured in the kinematical window $0.6 \le p_T \le 6$ GeV and in the limited rapidity region $|y| < 0.5$. In the QGSM we calculate the spectra integrated over p_T, so the direct comparison of our

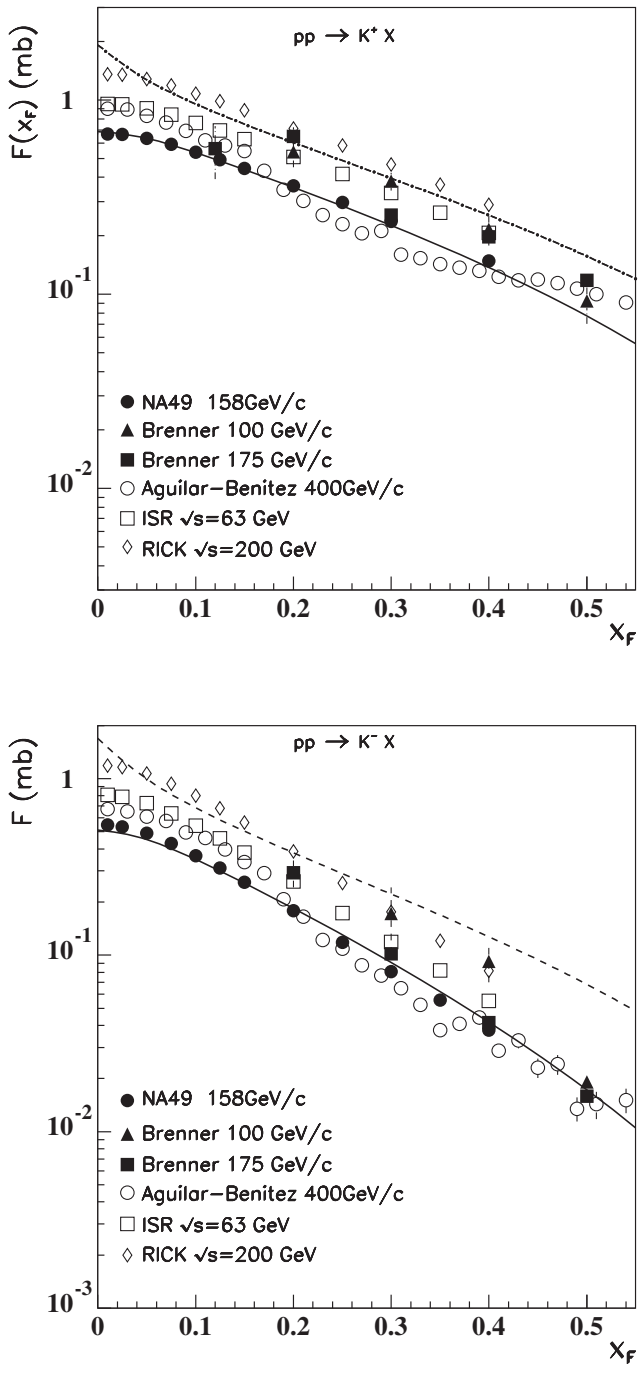

FIG. 6. The QGSM description of the invariant cross section of K^+ (upper panel) and K^- (lower panel) mesons produced in pp collisions compared to the experimental data at different energies [14,26,29]. Solid lines correspond to the QGSM result at 158 GeV/c ($\sqrt{s} = 17.3$ GeV), while dashed lines correspond to the QGSM calculation at RHIC energy ($\sqrt{s} = 200$ Gev).

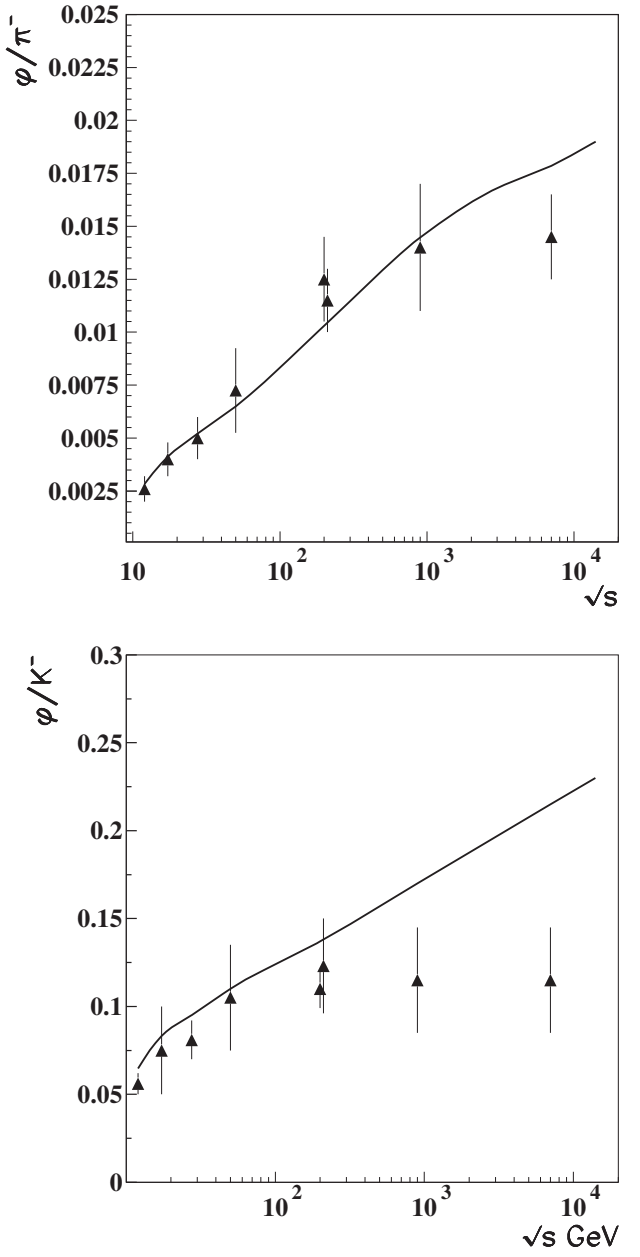

FIG. 7. The QGSM description of the $\sqrt{s}$ dependence of φ/π^- (upper panel) and φ/K^- (lower panel) cross section ratios produced in pp collisions, compared to the corresponding experimental data in Refs. [30–32].

calculations to the data would be inconsistent. The influence of the Kinematical boundaries at relatively low p_T should be at least in part smaller when we consider the ratios φ/π^- or φ/K^- with the same kinematical restrictions.

The energy dependence of the production cross section ratios of φ/π^- (upper panel) [30,31] and φ/K^- (lower panel) [30,32] in pp collisions are presented in Fig. 7, where the corresponding QGSM description is shown by solid curves. The energy dependences of our curves for φ/π^- and φ/K^- are similar, since the ratio of K/π production depends rather weakly on the initial energy.

One can see some disagreements of our curves with the data at high LHC energies. The predicted ratios for φ/π^- and φ/K^- increase from $\sqrt{s} = 0.9$ TeV to $\sqrt{s} = 7$ TeV, whereas at the experimental values they are practically the same. This disagreement could be explained if the experimental limits for the measured ratios were established not for rapidity y, but for the pseudorapidity η variable.

IV. CONCLUSION

The QGSM provides a reasonable description of Feynman x_F and rapidity y spectra of φ-meson production for the interaction of different hadron beams with a nucleon target in a wide energy region, by using for the only unknown parameter in our analysis, the normalization parameter a_φ, the value $a_\varphi = 0.11$. We show the QGSM prediction for dn/dy cross sections for LHC energies. We have also obtained a reasonable agreement for the φ/π^- and φ/K^- cross section ratios in a wide interval of the beam energy, going up to the LHC range. Since the theoretical ratios φ/π^- and φ/K^- grow with energy from $\sqrt{s} =$ 900 GeV to 7 Tev, while the experimental points do not show this growth, and, since, in particular, our prediction for the ratio φ/π^- at $\sqrt{s} = 900$ GeV is in agreement with the experiment, some discrepancy of our calculations with the experimental data appears at the LHC energy of $\sqrt{s} = 7$ TeV.

ACKNOWLEDGMENTS

We thank C. Pajares for useful discussions. We are also grateful to N. I. Novikova for technical help. This paper was supported by the Ministerio de Economía y Competitividad of Spain (Project No. FPA2011-22776), the Spanish Consolider-Ingenio 2010 Programme CPAN (Project No. CSD2007-00042), by Xunta de Galicia, Spain (Project No. 2011/PC043), by the State Committee of Science of the Republic of Armenia (Grant-13-1C023), and by the Russian Science Foundation (RSCF), through Grant No. 14-22-00281.

APPENDIX: QUARK AND DIQUARK DISTRIBUTIONS IN HADRONS IN QGSM

The QGSM considers hadrons as consisting of constituent quarks, so we cannot use hadron structure functions obtained from hard processes. Usually, it is assumed in DTU that a proton consists of a valence quark q and a diquark qq. The diquark qq contains not only two valence quarks, but also some part of gluon field, in what is called string junction (SJ) [33,34]. In this case, the diquark average momentum is larger than twice the momentum of a valence quark. In the QGSM a proton can also contain several sea quark-antiquark pairs.

In QGSM the form of the functions $u(x, n)$ is determined by the corresponding Regge asymptotic behaviors in the regions $x \to 0$ and $x \to 1$ [20,21]. As an example, let us consider the diagram with annihilation of one quark from the fast nucleon on a meson target, that is shown in Fig. 8(a).

The contribution of this process to the total inelastic hN cross section is proportional to $e^{[\alpha_R(0)-1]\Delta y}$, where $\alpha_R(0) \simeq 0.5$ is the intercept parameter of the corresponding nonvacuum Regge trajectory, and Δy is the difference between the rapidities of the colliding particles. On the other hand, and starting from the parton model, we can consider this process from a different point of view [21]; i.e., a slow valence quark exists in the incident fast nucleon that is Δy rapidity distant away from the valence diquark, the probability of such a configuration being equal to $V(\Delta y)$. This slow valence quark annihilates with a target antiquark with a rather large probability, what corresponds to the cut of the diagram in Fig. 8(a). Thus, the probability to find a slow valence quark in the fast nucleon at a distance Δy, i.e., with $x \simeq e^{-\Delta y} \to 0$ is equal to

$$x u_q(x) \sim x^{1-\alpha_R(0)}, \qquad x \to 0. \tag{A1}$$

The probability of finding a valence quark with $x \to 1$ in the nucleon is determined by the probability of finding a slow diquark. This can be detected in the process of $N\bar{N}$ annihilation that is shown in Fig. 8(b). The intercept of the corresponding Regge trajectory $\alpha_{qq\bar{q}\,\bar{q}}$ can be calculated as [21] $\alpha_{qq\bar{q}\,\bar{q}}(0) = -\alpha_R(0) + 2\alpha_B(0)$, where $\alpha_B(0) \simeq -0.5$ is a parameter of the nucleon Regge trajectory. Then,

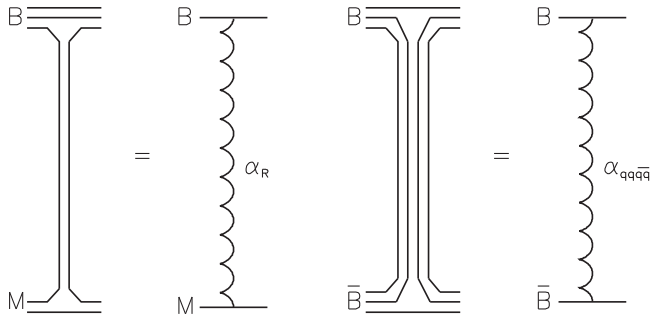

FIG. 8. Planar diagrams which determine the low-x asymptotic behavior of (a) the valence quark distribution and (b) of the diquark distribution in a nucleon.

$$xu_q(x) \sim (1-x)^{1+\alpha_R(0)-2\alpha_B(0)}, \qquad x \to 1. \tag{A2}$$

The quark distribution in the intermediate x region can be estimated with the help of a simple interpolation,

$$u(x) = Cx^{\alpha}(1-x)^{\beta}, \tag{A3}$$

with both limits at $x \to 0$ and $x \to 1$ given by Eqs. (A1) and (A2). The normalization factor C is determined by the condition

$$\int u_i(x,n)dx = 1, \tag{A4}$$

leading to

$$C = \frac{\Gamma(\alpha+\beta+2)}{\Gamma(\alpha+1)\Gamma(\beta+1)}. \tag{A5}$$

The numerical calculations account for the fact that the distribution of valence d-quark in the proton is softer than the distribution of valence u quarks. This can be done by including into $u_d(x,n)$ an additional factor $(1-x)$ with respect to $u_u(x,n)$. The diquark distributions can be derived from the quark distributions by substituting $x \to (1-x)$.

As a consequence of momentum conservation, for each value of n we have

$$\sum_i \langle x_i \rangle = \sum_i \int u_i(x,n)xdx = 1. \tag{A6}$$

In the case of $n > 1$, i.e., for multi-Pomeron exchange, the distributions of valence quarks and diquarks are softened with respect to the case of $n > 1$, due to the appearance of a sea quark contribution. For arbitrary n, one has [35]

$$\begin{aligned}
u_{uu}(x,n) &= C_{uu}x^{\alpha_R-2\alpha_B+1}(1-x)^{-\alpha_R+\frac{4}{3}(n-1)},\\
u_{ud}(x,n) &= C_{ud}x^{\alpha_R-2\alpha_B}(1-x)^{-\alpha_R+n-1},\\
u_u(x,n) &= C_u x^{-\alpha_R}(1-x)^{\alpha_R-2\alpha_B+n-1},\\
u_d(x,n) &= C_d x^{-\alpha_R}(1-x)^{\alpha_R-2\alpha_B+1+\frac{4}{3}(n-1)},\\
u_s(x,n) &= C_d x^{-\alpha_R}(1-x)^{\alpha_R-2\alpha_B+n-1}.
\end{aligned} \tag{A7}$$

The quark distributions in pion can be obtained in a similar way, e.g., for the case of π^- mesons, we use the distributions [35]

$$\begin{aligned}
u_d(x,n) = u_{\bar{u}}(x,n) &= C_d x^{-\alpha_R}(1-x)^{-\alpha_R+n-1},\\
u_u(x,n) = u_{\bar{d}}(x,n) &= C_u x^{-\alpha_R}(1-x)^{-\alpha_R+n-1}[1-\delta\sqrt{1-x}],\\
&\quad n > 1,\\
u_{\bar{s}}(x,n) &= C_{\bar{s}}x^{-\alpha_R}(1-x)^{n-1}, \qquad n > 1.
\end{aligned} \tag{A8}$$

[1] A. B. Kaidalov and K. A. Ter-Martirosyan, Yad. Fiz. **39**, 1545 (1984) [Sov. J. Nucl. Phys. **39**, 979 (1984)]; A. B. Kaidalov and K. A. Ter-Martirosyan, Yad. Fiz. **40**, 211 (1984) [Sov. J. Nucl. Phys. **40**, 135 (1984)].
[2] A. B. Kaidalov, Phys. At. Nucl., **66**, 1994 (2003).
[3] V. A. Abramovsky, V. N. Gribov, and O. V. Kancheli, Yad. Fiz. **18**, 595 (1973) [Sov. J. Nucl. Phys. **18**, 308 (1973)].
[4] A. B. Kaidalov and O. I. Piskounova, Yad. Fiz. **41**, 1278 (1985) [Sov. J. Nucl. Phys. **41**, 816 (1985)].
[5] Yu. M. Shabelski, Yad. Fiz. **44**, 186 (1986) [Sov. J. Nucl. Phys. **44**, 117 (1986)].
[6] G. H. Arakelyan, C. Merino, C. Pajares, and Yu. M. Shabelski, Eur. Phys. J. **C54**, 577 (2008); arXiv:0709.3174.
[7] C. Merino, C. Pajares, and Yu. M. Shabelski, Eur. Phys. J. **C71**, 1652 (2011).
[8] G. H. Arakelyan and Sh. S. Eremian, Yad. Fiz. **58**, 1321 (1995) [Phys. At. Nucl. **58**, 1241 (1995)].
[9] Sh. S. Eremian, Yad. Fiz. **59**, 144 (1996) [Phys. At. Nucl. **59**, 135 (1996)].
[10] G. H. Arakelyan, C. Pajares, and Yu. M. Shabelski, Z. Phys. **C73**, 697 (1997); arXiv:hep-ph/9602348.
[11] G. H. Arakelyan, A. Capella, A. B. Kaidalov, and Yu. M. Shabelski, Eur. Phys. J. **C26**, 81 (2002); arXiv:hep-ph/0103337.
[12] G. H. Arakelyan, A. B. Kaidalov, C. Merino, and Yu. M. Shabelski, Phys. At. Nucl. **74**, 426 (2011); arXiv:1004.4074.
[13] A. B. Kaidalov, Yad. Fiz. **45**, 1452 (1987) [A. B. Kaidalov Sov. J. Nucl. Phys. **45**, 902 (1987)].
[14] S. V. Afanasiev *et al.* (NA49 Collaboration), Phys. Lett. B **491**, 59 (2000).
[15] K. A. Ter-Martirosyan, Phys. Lett. **44B** (1973) 377.
[16] K. A. Ter-Martirosyan, Yad. Fiz. **10**, 1047 (1969) [Sov. J. Nucl. Phys. **10**, 600 (1970)].
[17] M. Froissart, Phys. Rev. **123**, 1053 (1961).
[18] A. M. Lapidus, V. I. Lisin, K. A. Ter-Martirosyan, and P. E. Volkovitsky, Yad. Fiz. **24**, 1237 (1976) [Sov. J. Nucl. Phys. **24**, 648 (1976)].
[19] G. Atchem *et al.* (TOTEM Collaboration), Europhys. Lett. **96**, 21002 (2011).
[20] A. Capella, U. Sukhatme, and J. Tran Thanh Van, Z. Phys. **C3**, 329 (1980).
[21] A. B. Kaidalov, Z. Phys. **C12**, 63 (1982).

[22] C. Daum *et al.*, Nucl. Phys. **B186**, 205 (1981).
[23] H. Dijkstra *et al.* (ACCMOR Collaboration), Z. Phys. C **31**, 375 (1986).
[24] R. J. Apsimon *et al.* (Omega-Photon Collaboration), Z. Phys. C **61**, 383 (1994); F.-D. Gebert, Report No. Bonn-IR-92-10 (1992) (in German).
[25] M. Aguilar-Benitez *et al.* (LEBC-EHS Collaboration), Z. Phys. C **44**, 531 (1989).
[26] T. Anticic *et al.* (NA49 Collaboration), Eur. Phys. J. **C68**, 1 (2010).
[27] M. Atayan and H. Gulkanyan, arXiv:hep-ex/0501024.
[28] M. Aguilar-Benitez *et al.* (LEBC-EHS Collaboration), Z. Phys. C **50**, 405 (1991).
[29] A. E. Brenner *et al.*, Phys. Rev. D **26**, 1497 (1982).
[30] J. Adams *et al.* (STAR Collaboration), Phys. Lett. B **612**, 181 (2005); arXiv:nucl-ex/0406003.
[31] B. Abelev *et al.* (ALICE Collaboration), Phys. Lett. B **710**, 557 (2012); arXiv:1112.2082.
[32] B. Abelev *et al.* (ALICE Collaboration), Eur. Phys. J. **C72**, 2183 (2012); arXiv:1208.5717.
[33] M. Imachi, S. Otsuki, and F. Toyoda, Prog. Theor. Phys. **54**, 280 (1975); **55**, 551 (1976).
[34] G. C. Rossi and G. Veneziano, Nucl. Phys. **B123**, 507 (1977).
[35] A. B. Kaidalov, K. A. Ter-Martirosyan, and Yu. M. Shabelski, Yad. Fiz. **43**, 1282 (1986); [Sov. J. Nucl. Phys. **43**, 822 (1986)].